

Modeling and Reproducibility of Suzaku HXD PIN/GSO Background

Yasushi FUKAZAWA¹, Tsunefumi MIZUNO¹, Shin WATANABE²,
Motohide KOKUBUN², Hiromitsu TAKAHASHI¹,
Naomi KAWANO¹, Sho NISHINO¹, Mahito SASADA¹, Hirohisa SHIRAI¹,
Takuya TAKAHASHI¹, Tomonori YAMASAKI¹, Tomonori YASUDA¹, Aya BAMBA²,
Masanori OHNO², Tadayuki TAKAHASHI², Masayoshi USHIO², Teruaki ENOTO³,
Takao KITAGUCHI³, Kazuo MAKISHIMA^{3,4}, Kazuhiro NAKAZAWA³, Yuichi UEHARA³,
Shin'ya YAMADA³, Takayuki YUASA³, Naoki ISOBE⁴, Madoka KAWAHARADA⁴,
Takaaki TANAKA⁵, Makoto TASHIRO⁶, Yukikatsu TERADA⁶, and Kazutaka YAMAOKA⁷

¹*Department of Physical Science, Hiroshima University, 1-3-1 Kagamiyama,
Higashi-Hiroshima, Hiroshima 739-8526
fukazawa@hirax7.hepl.hiroshima-u.ac.jp*

²*Department of High Energy Astrophysics, Institute of Space and
Astronomical Science (ISAS), Japan Aerospace Exploration Agency (JAXA),
3-1-1 Yoshinodai, Sagamihara, Kanagawa 229-8510*

³*Department of Physics, University of Tokyo, 7-3-1 Hongo, Bunkyo, Tokyo 113-0033*

⁴*Cosmic Radiation Laboratory, The Institute of Physical and Chemical Research (RIKEN),
2-1 Hirosawa, Wako, Saitama 351-0198*

⁵*SLAC National Accelerator Laboratory and KIPAC, Stanford University, Menlo Park, CA, USA*

⁶*Department of Physics, Saitama University, 255 Shimo-Ohkubo, Saitama-City, Saitama 338-8570*

⁷*Department of Physics, Aoyama Gakuin University, 5-10-1 Fuchinobe, Sagamihara, Kanagawa 229-8558*

(Received 2007 0; accepted 2008 0)

Abstract

Suzaku Hard X-ray Detector (HXD) achieved the lowest background level than any other previously or currently operational missions sensitive in the energy range of 10–600 keV, by utilizing PIN photodiodes and GSO scintillators mounted in the BGO active shields to reject particle background and Compton-scattered events as much as possible. Because it does not have imaging capability nor rocking mode for the background monitor, the sensitivity is limited by the reproducibility of the non X-ray background (NXB) model. We modeled the HXD NXB, which varies with time as well as other satellites with a low-earth orbit, by utilizing several parameters, including particle monitor counts and satellite orbital/attitude information. The model background is supplied as an event file in which the background events are

generated by random numbers, and can be analyzed in the same way as the real data. The reproducibility of the NXB model depends on the event selection criteria (such as cut-off rigidity and energy band) and the integration time, and the 1σ systematic error is estimated to be less than 3% (PIN 15–40 keV) and 1% (GSO 50–100 keV) for more than 10 ksec exposure.

Key words: instrumentation: detectors — methods: data analysis — X-rays: general

1. Introduction

The hard X-ray detector (HXD)(Takahashi et al. 2007; Kokubun et al. 2007) onboard Suzaku (Mitsuda et al. 2007) has been developed to enable observations of astronomical objects with a good sensitivity in the 10–600 keV band. When the HXD data are combined with the data from the X-ray CCD camera (XIS), they simultaneously cover a wide energy band, from 0.2 keV to 600 keV. The HXD sensor part (HXD-S) consists of 64 Si-PIN photo diodes and 16 GSO/BGO phoswich counters, shielded by 20 BGO anti-coincidence counters. Such a compound-eye configuration greatly reduces the background and the dead-time. Each of the phoswich counter (well counter) units includes 4 Si-PIN photo diodes with 2 mm thickness and 4 GSO scintillators with 5 mm thickness, located at the bottom of the BGO well-shaped active collimator. The HXD is the first astronomical detector to utilize such thick Si-PIN diodes and high-Z GSO scintillators. In order to achieve lower background level than any other previous missions, the HXD has been designed to contain less radio isotopes – which may be naturally contained in the detector or activated in the orbit – and reject the background events very effectively. The important goal of the HXD is the achievement of the low background level by rejecting particle background and Compton-scattered events as much as possible. It is found that, considering the detection efficiency, the residual background level of the HXD is achieved to be 10 mCrab at 20 keV and 1 Crab at 200 keV, the lowest of all previous missions, such as BeppoSAX and RXTE. Such a low background level enables us to detect weak sources of several hundreds μ Crab in several tens keV band or several mCrab around 100 keV, without a necessity for the “rocking motion” of the detector for simultaneous monitoring of the background, as has been done with CGRO/OSSE, BeppoSAX/PDS, and RXTE/HEXTE.

Such a low background level and narrow field of view are unique in order to permit the detection of faint hard sources, give less source confusion and contribution of the Cosmic X-ray Background, and provide a rudimentary capability to study the structure for the emission region of hard X-rays, especially for supernova remnants, galactic diffuse X-ray emission, and galaxy clusters. Simultaneous observations with the XIS CCD camera – with no gap in the spectral coverage – are very effective to constrain the time variability of the broad-band spectrum, and

the appreciable effective area up to several hundred keV enables us to determine the continuum shape accurately, which is especially important for time-variable Galactic binaries and active galaxies.

Although the HXD achieved the low background level, the count rate of the background significantly varies with time, depending on mainly two parameters; geomagnetic cut-off rigidity (COR) and elapsed time after passages of the South Atlantic Anomaly (SAA), but weak dependences on other parameters such as earth elevation are found. Therefore, the NXB must be estimated by taking into account these dependences. Since the sensitivity is limited by the reproducibility of the NXB, a correct NXB model is strongly required. The HXD team has developed the NXB model with several different methods and unified them by combining advantages of each method. Here we report the HXD background modeling and its reproducibility. Corresponding Suzaku documents are also available on the Suzaku web site as Suzaku memo¹ 2007-01, 2007-02, 2007-09, 2008-01, and 2008-03. In this paper, some technical terms often appear and therefore we summarize them in table 1.

2. Characteristics of HXD NXB

Here we show the characteristics of the HXD NXB. We utilize the data during the earth occultation, which are almost equivalent to the NXB. The earth albedo is at most 10 % of the CXB flux below 50 keV (Imhof et al. 1976; Churazov et al. 2007; Frontera et al. 2007; Sazonov et al. 2007; Churazov et al. 2008), and the CXB flux is 5% of the PIN NXB and <0.5% of the GSO NXB.

2.1. Summary of the NXB Components

Detail description of the HXD NXB is written in Kokubun et al. (2007). Here we shortly review it, and present the characteristics which has been newly found. Example of light curves of the HXD background is shown in figure 1. The HXD background events are mainly caused by natural radio active isotopes, SAA-induced radio isotopes, primary and secondary cosmic rays, and atmospheric albedo neutrons. Therefore, the count rate of the background significantly varies with time, depending on mainly two parameters. First is the dependence of the COR for primary cosmic rays and atmospheric neutrons. This dependence is well tracked by PINUD, which counts the upper discriminator signal of the PIN at the threshold energy of ~ 90 keV. Therefore, the PINUD is insensitive to X-ray events, but monitors a flux of real-time charged particles. Since the PIN diodes are embedded in the thick BGO shields, PINUD counts the proton above ~ 100 MeV. This component is dominant in the variation of PIN NXB and GSO NXB below 140 keV. The spectra of PIN NXB become harder as the COR decreases or the PINUD increases. The PINUD is considered to be a better indicator of the particle flux than the COR, because the particle environment against the COR would depend on the

¹ <http://www.astro.isas.jaxa.jp/suzaku/doc/>

solar activity. The second is exponential-decay components after passages of SAA, due to the activated material bombarded by SAA protons, which is monitored by the hit count of PINUD integrated during the SAA (thus representing the total accumulated dose). This component is significant in the GSO band below 100 keV and above 400 keV, while the variation due to this component is smaller for the PIN NXB. Since there are many activated nuclides with different life times, many time scales of NXB variation also exist in the range of several seconds to several hundred days. These two dependences are the clearest, but other weak dependences have been found. For example, the background rate is somewhat dependent on whether the pointing direction is toward the sky or the earth. Details are described later in §3.2.3.

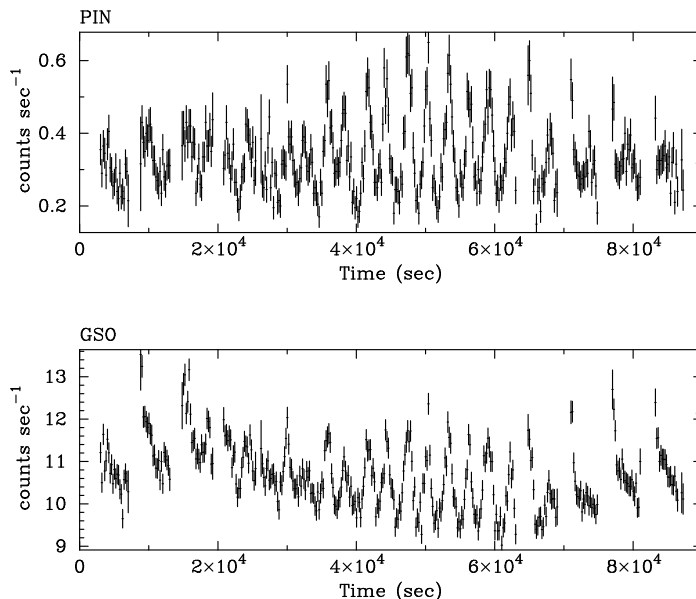


Fig. 1. Left and right show examples of light curves of the PIN (15–40 keV) and GSO (50–200 keV) background, respectively. The variation of COR-dependence is seen at 2×10^4 – 6×10^4 sec, and exponential-decay components after passages of SAA are seen at 0 – 2×10^4 sec and after 6×10^4 sec.

2.2. HXD Operation and NXB

Apart from the intraday variation, the count rate of the NXB depends on the HXD operation mode and the activation of detector material with long life times. There has been two kinds of important changes of the HXD operation mode. The lower discrimination level and pulse-shape discrimination level for the GSO signal determines the background rejection efficiency of PIN NXB, and therefore their level change can cause the change of the PIN NXB. Due to the noise increase of one PIN possibly caused by the in-orbit radiation damage, the bias high voltage to the PIN was changed twice. Since the thickness of depletion layer depends on the bias, this change slightly affected the energy response of the 16/32 PIN and thus PIN NXB rate might also be affected. Therefore, the response matrices corresponding to different

Table 1. Acronym.

HXD	Hard X-ray Detector
PIN	p-i-n type Si photo diode in the HXD
GSO	GdSiO scintillator in the HXD
BGO	BiGdO anti-coincidence scintillator in the HXD
BGD	background
CXB	Cosmic X-ray background
NXB	non X-ray background
SAA	South Atlantic Anomaly
PINUD	PIN Upper discriminate counter
PINUD _{buildup}	convolution of PINUD with an exponential decay function
COR	geomagnetic cut-off rigidity
PINUDLCUNIT (bgd _l a or quick)	background model (§3.1)
LCFITDT (bgd _l a or tuned)	background model (§3.2)
LCFIT	background model (§3.2)
GSOHCNT	count rate of GSO event in 450–700 keV
GLC	gradually increasing component of the GSO background event in 450–700 keV
T_SAA_HXD	elapsed time after the SAA

bias voltages were supplied from the HXD team. The activation due to long-lived radio-active nuclei leads to the increase of the NXB rate, especially for the GSO.

Here we show the long term variation of the NXB, concerning the above issues. Figure 2 top shows a two-year history of the PIN NXB count rate (15–40 keV) during earth occultation data. The count rate is almost constant, and thus the activation is not important for the PIN NXB. However, some discrete or gradual changes are seen; the most significant are two discrete jumps around a day of 260 and 310. This is due to the above level changes for the GSO on 2006 March 23 and May 13. Bias voltages for 16 out of 64 PIN were reduced from 500 V to 400 V on 2006 May 29 (323 days after the launch), and those of additional 16 PIN down to 400 V on 2006 Oct 3 (450 days after the launch). Nevertheless, we find no significant changes of the PIN NXB rate from this figure. Apart from those variations, the PIN NXB rate will suffer the increase of solar activity in the near future.

In figure 2 bottom, a two-year history of the GSO count rates of the NXB in 50–200 keV during earth occultation data is plotted. Due to the activation of long-lived nuclides during the SAA passage, the count rate gradually increases and is reaching saturation. The increase is larger in the lower energy band. Figure 3 shows the comparison of spectra of earth occultation data in different epochs. Gradual increase of several activation-induced lines are clearly seen.

During 2006 March 14 to May 13 (247–307 days after the launch), observational mode for the GSO had been changed several times to optimize the setting parameters before the guest observer program started. The GSO count rate below 100 keV, especially around the lower disc level, was affected by these mode changes. Although this affection is significant but small, it is not clearly seen in figure 3. As a result, the background model should consider these issues.

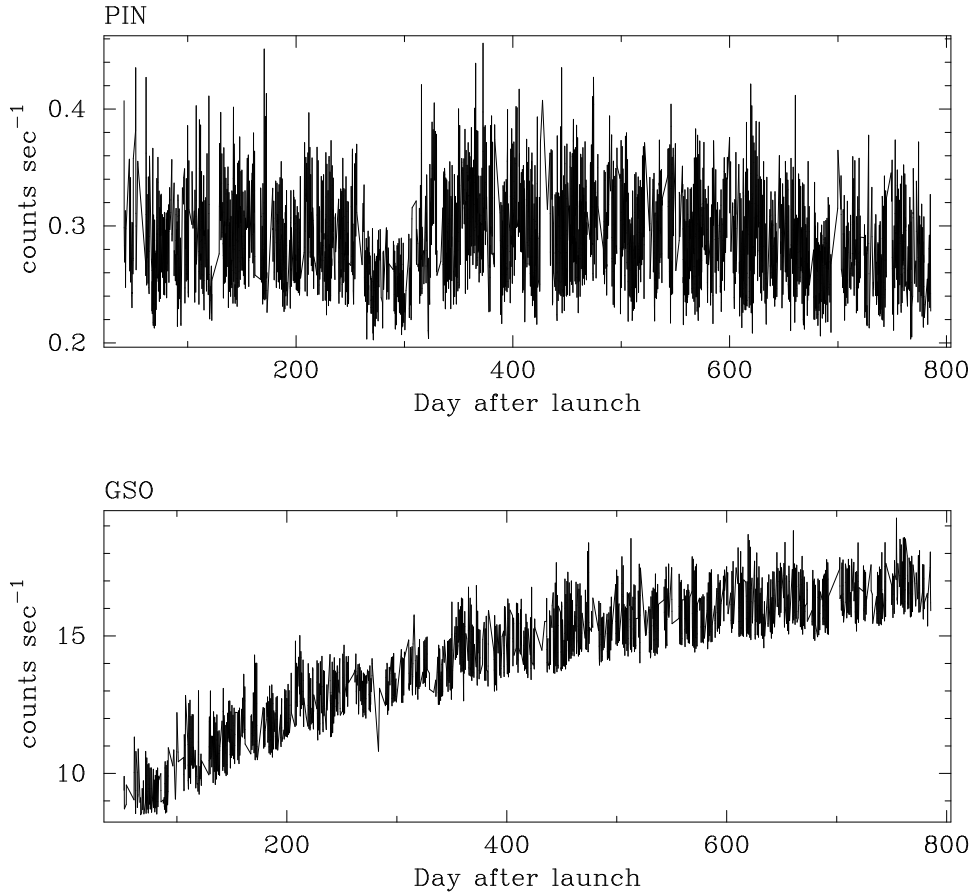


Fig. 2. Time history of the PIN count rate (15–40 keV) (top) and the GSO count rate (50–200 keV) (bottom) of NXB during earth occultation data. The period of low count rate of the PIN NXB corresponds to 2006/03/23 – 2006/05/13 (day from launch = 256 – 307).

3. Modeling of NXB

The most ideal model of the NXB is based on the first principle; predicting the NXB count rate by considering the orbital particle environment and the detector response correctly, for example, by Monte-Carlo simulations. We in fact predicted the GSO background level due to the activation by Monte-Carlo simulations (Kokubun et al. 1999; Kokubun et al. 2007)

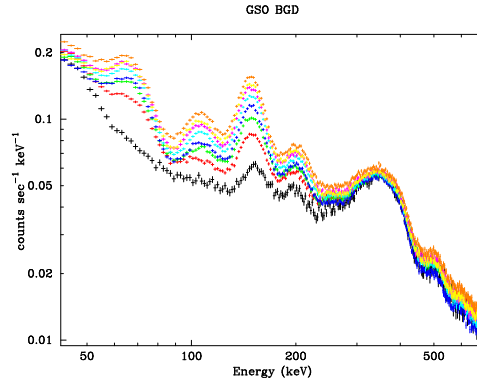


Fig. 3. Comparison of the GSO NXB spectra using earth occultation data in different epochs; 2005-08-31, 2005-12-03, 2006-03-09, 2006-06-13, 2006-09-26, 2007-01-05, 2007-04-10, and 2007-08-09 from bottom to top.

within a factor of 2. However, in order to reproduce the NXB with a few % accuracy, it is more realistic to utilize the actually observed NXB. In that case, there are usually two types of methods.

One is based on the NXB data base which is sorted by some parameters, such as COR, and the NXB for the observation is constructed by referring to parameters to extract the data base. This method is available when the number of sorting parameters are at most two; the NXB time variation is not so complex. Furthermore, it is needed that the background properties, which would depend on other parameters than sorting parameters, do not change within the period during which the NXB data base is accumulated. The background model of the Suzaku XIS applies this method (Tawa et al. 2008). However, strictly speaking, the NXB usually depends on more than two parameters, and therefore the accuracy of this method is somewhat limited.

The second method is to predict the NXB by the empirical function which represents the NXB time variation by several parameters. The function is constructed through the analysis of the real time variation of the NXB. The background models of the Ginga LAC and the RXTE PCA are based on this method (Hayashida et al. 1989; Jahoda et al. 2006). This method can include many parameters to represent the function, but enough statistics of the NXB is necessary to track the time variation of NXB with a time scale of several hundred seconds. In the case of low count rate of NXB, it is somewhat difficult to find modeling parameters.

The count rate of the PIN NXB is not so high but enough to utilize the second method, while that of the GSO NXB is high and more variable. The latter method is more accurate, but cannot prepare the NXB model just after the data becomes available, while the former method can prepare the NXB model quickly. Therefore, we developed the PIN NXB model using both methods and the GSO NXB model using only the latter one. The model background is supplied as an event file by generating the background event by random numbers, and can be analyzed in the same way as the real event file.

3.1. *Method based on the data base sorted by PINUD and PINUD build-up : PINUDLCUNIT (PIN NXB model)*

The method described here utilizes the two-parameter-sorted database, and is applied to the PIN NXB model. In this method (PINUDLCUNIT)², the NXB model is constructed on the data base of the earth occultation data. The real time PINUD count rate can be used as a good indicator of the NXB component. Another NXB component related with the activation cannot be modeled by simply using PINUD. Therefore, we introduced a parameter “PINUD build-up”, which is a convolution of PINUD with an exponential decay function, represented by

$$\text{PINUD}_{\text{buildup}}(t) = \int_{-\infty}^t \text{PINUD}(t_0) \exp\left(-\frac{t_0 - t}{\tau}\right) dt_0$$

Various values of time constant τ was tried between 5000–10000 sec and $\tau = 8000$ sec was selected in the latest model. Typical light curves of PINUD and $\text{PINUD}_{\text{buildup}}$ are shown in figure 4.

Then, PINUD and $\text{PINUD}_{\text{buildup}}$ are utilized to sort and refer to the earth occultation data base. We accumulated PIN event data and pseudo event data (for dead time correction) under the conditions that the target elevation angle from the earth limb should be $< -5^\circ$. Since the PIN NXB count rate was affected by the change of bias voltages (500V to 400V) and there is a gradual variation of the NXB, the data base is accumulated by considering these issues. There are 16 well unit counters in the HXD, each of which contains 4 PIN diodes. Since the NXB variation is somewhat different among units (Kokubun et al. 2007), the data base of each unit is sorted and referred to PINUD and $\text{PINUD}_{\text{buildup}}$ of the corresponding unit. The data base consists of 40×220 PIN NXB spectra and pseudo events for 4 PINs in each unit. The range of the PINUD in the data base is from 2.5 cts sec^{-1} to $42.5 \text{ cts sec}^{-1}$ per one unit, and that of the $\text{PINUD}_{\text{buildup}}$ is from $4.0 \times 10^4 \text{ cts}$ to $2.25 \times 10^6 \text{ cts}$ per one unit. Figure 5 presents an example of the NXB data base divided into four energy bands for the visualization. It has been found that the long-term variation of the PIN NXB is significant and it is not so well reproduced by the data base prepared as above. Therefore we correct the total PIN NXB count rate in the data base by a 2nd order polynomial function of time.

The PIN NXB for each observation is estimated by picking up a spectrum from the data base, based on the two parameters. The reference to the data base is performed at each sampling rate of PINUD (2, 4, 8, or 32 sec). The exposure of the picked-up spectrum is corrected with dead-time. A time to the next event is determined by the Poisson statistics, based on the total count rate of the NXB spectrum. In order to reduce the statistical error of the number of events in the PIN NXB model, we apply 10 times as high a PIN background rate as the prediction. A pulse height is obtained by generating random numbers which follow the referred spectrum

² It is referred as “quick” or “bgd_a” in the Suzaku team. The event FITS files generated with this method are identified by the keyword of PINUDLCUNIT in the METHOD record of the FITS file header.

as a probability distribution. These processes are repeated until the event time passes the end time of each PINUD sampling period, and the process goes to the event generation in the next PINUD sampling period.

This method can generate the NXB model as soon as possible, after the PINUD history becomes available. Therefore, the HXD team supplies the NXB model of this method quickly so that observers can start the analysis at the same time as the data become available. Note that this modeling is not available for the data from 2006 March 23 to 2006 May 13, because of the systematic change of the PIN-NXB count rate as described in §2.

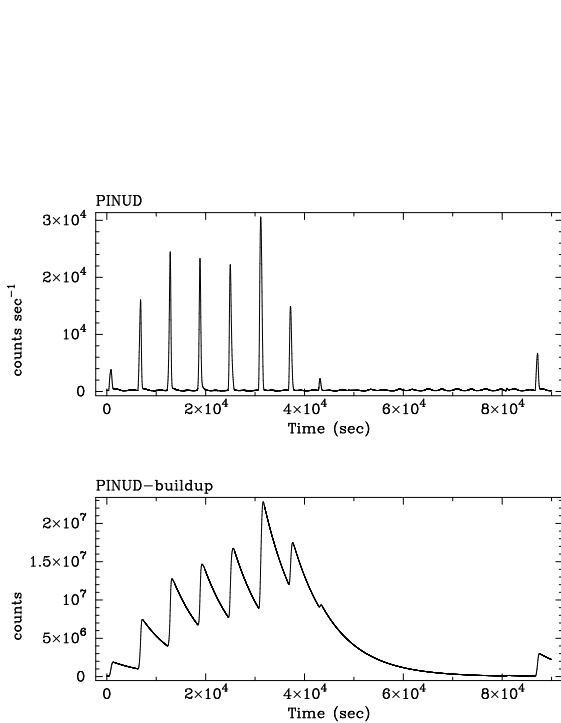


Fig. 4. Example of PINUD-buildup. Top panel shows the light curve of the PINUD count rate in unit of cts sec^{-1} per one unit (4 PINs), and bottom shows the $\text{PINUD}_{\text{buildup}}$ convolved with a time constant of 8000 sec.

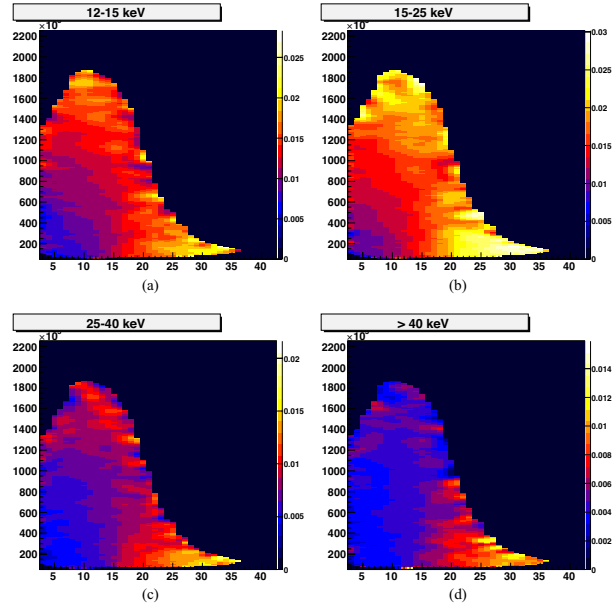


Fig. 5. A NXB database of the PINUDLCUNIT method for (a) 12–15 keV, (b) 15–25 keV, (c) 25–40 keV, and (d) >40 keV. The horizontal and vertical axes are PINUD and $\text{PINUD}_{\text{buildup}}$, respectively. Color represents the count rate of the PIN NXB.

3.2. Method based on Parameterization of background light curve : LCFITDT (*PIN/GSO NXB model*)

The GSO NXB exhibits much stronger variations as a result of activation induced during the SAA passages. These variations are strongly energy-dependent, because many activated nuclei emit various gamma-ray lines together with the continuum. Since the method of simply using the parameter-sorted data base is very difficult to model the GSO NXB, an alternative method is developed, which directly fits the NXB light curves with an empirical model, determines its parameters, and predicts the NXB count rate at any given time. Note that this

modeling (LCFITDT)³ can be applied to the PIN NXB as well. In order to reproduce the energy dependence of the background light curve, we model the background separately in 32 energy bands for the GSO NXB. On the other hand, the low count rate of the PIN NXB does not allow us to study the energy dependence of the light curve in detail, and thus we at first model the light curve in 12–70 keV band and distribute the count rate in a single 12–70 keV band into 256 energy channels, based on the data base of PIN NXB spectral shapes which are sorted by COR⁴ and T_SAA_HXD (elapsed time after SAA). However, PIN NXB spectral change would depend on other parameters than the above two parameters, but it is found that the dependence is too small to recognize in the early phase due to low event statistics of PIN NXB, especially for the higher energy band. Therefore, we included such effects after the first-version modeling function is constructed and studied (§3.2.3).

Since the modeling needs the complete PINUD history and the reprocessed gain-calibrated GSO data, the GSO reprocess becomes available after the release of the gain history file for the corresponding observation date, and it is usually 1.0–1.5 months after the pipeline processing. Therefore, the NXB model with the LCFITDT method is released after 1.5–2.0 months after the pipeline processing, unlike the PINUDLCUNIT method.

3.2.1. Parameterization of the NXB model

In order to study the time variation of the NXB, we accumulate the earth occultation data, under the following conditions. The target elevation angle should be $< -5^\circ$ (namely, during the Earth occultation); the data rate of the Satellite Data Processor (DP) should not be low (L); the in-orbit HXD data transfer should not be saturated; and the COR should be > 6 GV. For the GSO, we divide the accumulated events into 32 energy bands, and derive 200-sec bin light curves in each energy band. Boundaries of the 32 energy bands are logarithmically spaced from 53 keV to 1024 keV, with each band having a typical BGD rate of 0.5–1 cts sec⁻¹. The PIN light curve is analyzed in a single 12–70 keV energy band.

After the 32 GSO NXB light curves and one PIN NXB light curve are prepared, we fit them individually, with an empirical model to be constructed in the following manner. Like in the modeling method PINUDLCUNIT, the PINUD dependence is represented by a term which is a second order polynomial function of the PINUD counts summed over the 64 PIN diodes. Likewise, the activation component is represented by PINUD build-up counts. In this model, several exponential decay functions with different time constants τ_k are considered. The convolution integral is calculated up to $30\tau_k$, in order to save the calculation time.

Various studies indicate that we need at least 3 or 4 time constants, τ_k , to represent the build-up effects in each energy band. In order to find them, we performed a preliminary

³ This method is referred as “tuned” or “bgd_d” in the Suzaku SWG team. The event FITS files generated with this method are identified by the keyword of LCFIT or LCFITDT in the METHOD record of the FITS file header. Both are basically the same method, but the former does not include the dead-time correction.

⁴ Here we do not use the PINUD, because of technical convenience.

analysis. That is, we fitted a whole light curve of the Earth occultation data acquired in the period from 2005 September 2 to 2006 February 28. with a model consisting of the second order polynomial function of the PINUD counts and the PINUD build-up term with two time constants. Then, we produced confidence contours for the two time constants by scanning them independently. First, we scanned the two time constants in a range shorter than one day, and determined them. After fixing these two short time constants, we newly added two build-up time constants longer than one day, and repeated the search. A shorter time constant was scanned at grid values of 0.5, 0.8, 1.0, 1.5, 2.0, 2.5, 3.0, 4.0, 5.0, 7.0, 10.0, 13.0, 15.0, 18.0, 22.0, 30.0, 45.0, 60.0, 80.0, and 100 ksec, while a longer one is scanned over 0.15, 0.25, 0.35, 0.45, 0.55, 0.8, 1.0, 2.0, 3.0, 5.0, 6.5, 8.0, 10.0, 20.0, and 30.0 Msec. Thus, we have obtained 4 time constants that describe the PINUD build-up effects in each energy band. The obtained four time constants are typically 1–2 ksec, 10–20 ksec, a few days, and several tens days, depending on the energy band.

While the activation effects have thus been described approximately by PINUD build-up with four time constants, the modeling is found to be incomplete, mainly due to the following two reasons. We have found that the activation BGD also depends on the angle θ_B between the geomagnetic field and the HXD field of view. When θ_B is small, the SAA particles directly enter the tight HXD shield “Wells”. As a result, the GSO background count rate due to the activation becomes higher even for the same entrance number of the SAA particles or PINUD build-up count (5–10% higher when the angle is around 0°). When we include this angle dependence, the background reproducibility was somewhat improved. Apart from the θ_B dependence, there might be other components of activation with time constants other than four time constants included in the model. Such components can be represented by real GSO NXB count rate. Then, we additionally consider the 450–700 keV GSO count rate, $GSOHCNT(t)$, where celestial signals in such energy band are negligible, less than 0.2% even during the Crab observation.

From the above consideration, the empirical model describing the light curve in the i -th energy band is expressed as

$$\begin{aligned}
BGD_i(t) = & a_i + \sum_{k=0}^3 b_{k,i} \int PINUD(t') \cdot \exp\left(-\frac{t-t'}{\tau_{k,i}}\right) dt' \\
& + \sum_{k=0}^3 c_{k,i} \left[\int \frac{90^\circ - \theta_B(t')}{90^\circ} \cdot PINUD(t') \cdot \exp\left(-\frac{t-t'}{\tau_{k,i}}\right) dt' \right]^p \\
& + d_i \cdot PINUD(t) + e_i \cdot PINUD^2(t) \\
& + f_i \cdot (GSOHCNT(t) - GLC(t)) \cdot \left[1 + g_i \exp\left(-\frac{t-t_{SAA}}{\tau_g}\right) \right] \\
& + h_i(t) \ ,
\end{aligned}$$

where the coefficients a_i , $b_{k,i}$, $c_{k,i}$, d_i , e_i , f_i , and g_i are model parameters to be adjusted, and t_{SAA} is the elapsed time from the end of the latest SAA, while $\tau_{k,i}$ are fixed to the values as

obtained above and τ_g are fixed to 10000 sec as described later. The index p is 1, except that it is 2 for two shorter time scales of the PIN NXB. The terms with the coefficients, $b_{k,i}$ and $c_{k,i}$, represent the activation, and the term with d_i and e_i does the PINUD dependence. The term with $f_{k,i}$ and g_i is included to reproduce the activation more accurately with $GSOHCNT(t)$. $GLC(t)$ is a gradually increasing function of the GSO count rate, and obtained by fitting the light curve of 450–700 keV band from 2005 Aug 17 to the current time by the PINUD-build up terms with two long time constants of 0.35 Msec, and 30 Msec. This function subtracts the long-term gradual increase from $GSOHCNT(t)$ so that the GSO count rate only represents the day-by-day background variation that cannot be fully reproduced by other model components. Furthermore, to consider the difference of the time constant of activation between 450–700 keV and other energy band, we include the exponential term with a time constant of $\tau_g = 10000$ sec, which is found to give a good reproducibility. The last term in this model, h_i , is a correction bias to be explained later, introduced in order to reduce the current uncertainty as much as possible. As a result, input data for modeling the background are $PINUD(t)$, $GSOHCNT(t)$, $\theta_B(t)$, and t .

3.2.2. Modeling Procedure of the GSO NXB

Here we describe the procedure of the GSO NXB modeling, based on the model function in §3.2.1. The procedure of the PIN NXB modeling is somewhat different, and thus we describe it in §3.2.3, especially for the specific issues.

A set of monthly model parameters are determined by fitting the light curve of the Earth occultation data from each month, together with those before and after 10 days of that month. Time region of each fit does not cross any occasion when the HXD operation mode (such as high-voltages and lower discriminator levels) was changed. After once performing the fit, we exclude data points with large deviations by $> 5\sigma$ (σ is a root-mean-square), and perform the fit again to obtain the final parameters. In the fitting, we fix the correction bias h_i to 0. Afterwards, we calculate the residual between the background and the model in every 150 ksec, and employ the residual as the correction bias h_i ; $h_i(t)$ varies every 150 ksec, while the other model parameters are constant in each month. Here we adapt 150 ksec, since residual in a shorter time scale picks up the Poisson fluctuation and one in a longer time scale smears out the residual profile. Typically, h_i is at most 0–2% of the total background. Currently, the number of parameters is still not optimized, and therefore parameter couplings in the light curve fitting sometimes introduce a small discontinuity of count rate in each component at the month boundary, but the discontinuity is canceled after adding each component.

After the BGD model parameter sets are thus determined for each energy band, we create the background light curve in each energy band at each PINUD sampling time. In this process, we correct the dead-time by using the dead-time light curve estimated from the HXD pseudo event ⁵. Finally, BGD events in each band are created, with their pulse heights

⁵ Currently, the GSO NXB model is not corrected by the dead-time, and thus we refer it as the LCFIT model,

determined by a Monte-Carlo method referring to the model-predicted counts in each PINUD sampling period. As shown in figure 6, the pulse height is uniformly and randomly distributed within each energy band of the GSO. Therefore, users should use exactly the same energy boundaries as the present model, when binning the GSO spectra.

3.2.3. Procedure of the PIN NXB modeling

The procedure to prepare the model of the PIN NXB light curve is the same as the GSO NXB, but for only one energy band. The correction factor $h_i(t)$ is also created in the same way as the GSO NXB model. In order to reproduce the PIN NXB spectrum, pulse height of each event is generated by random numbers, which follows probability distributions referring to the actual pulse-height spectral database, accumulated under various values in the COR and T_SAA_HXD; the database is sorted at boundaries of 6, 7, 8, 9, 10, 11, 12 GV in the COR, and 2000, 4000, 10000 sec with respect to T_SAA_HXD. The database is created from the earth occultation data during 100 days centering on each month, together with the condition that the observational set-up of the HXD is the same within each period.

Although we represent the energy-dependence of the PIN NXB light curve as described above, the modeling accuracy is limited because we consider only two parameters to reproduce the energy dependence. The PIN NXB count rate is dominated by events in lower energy band, and therefore the above modeling is relatively good for lower energy band, but the accuracy becomes worse toward the higher energy band. If the model shows systematic deviations from the real NXB data and the deviations can be modeled with some appropriate parameters, we can improve the reproducibility of the PIN NXB model. Figure 7 and 21 show an example of comparison of the NXB model with the earth data against the elevation angle from the earth rim, the COR, the satellite altitude, and the angle θ_B between the geomagnetic field and the Suzaku field of view. Here we averaged the earth occultation data from 2005 September to 2007 August. In the plot against the elevation angle, the blank sky data defined in §4 are used to cover the elevation above 0° . Systematic residuals of several % are clearly seen in these figures, but they can be recognized for the first time after long accumulation of the PIN NXB data, because of low count rate of the PIN NXB, especially in a higher energy band. The residuals against the COR are due to the incomplete modeling of the COR dependence by PINUD. Toward the higher satellite altitude, the residuals change positively or negatively in lower or higher energy band of the PIN NXB, respectively, probably because the particle environment becomes different along the altitude. Negative correlation is seen in the residual against the elevation in 40-70 keV band; the model tends to overestimate the NXB at larger elevation. Note that the jump at the elevation of 0° is due to the CXB signal above 0° . Since the earth albedo is at most 0.3 % of the PIN NXB, the elevation dependence cannot be explained by it. Perhaps this dependence is thought to be due to secondary particles created through

to distinguish the dead-time corrected PIN NXB model. In the near future, we will release the dead-time corrected LCFITDT GSO NXB model.

the interaction between primary cosmic rays and earth atmosphere, and intensity of secondary particles is somewhat higher from the earth side. The residual in 15–40 keV becomes larger for the θ_B around 30° and 150° , possibly because the effective thickness of the BGO active shield becomes the largest and the NXB becomes smaller for these incident directions.

Then, we corrected the above systematic dependences against the elevation, satellite altitude, COR, and θ_B . Residual profiles are obtained in the energy range of 15–25, 25–40, 40–70 keV and are fitted with a 3–5th order polynomial function of the corresponding parameter (COR, elevation ...). The correction factor for arbitrary energy is calculated by linear interpolation between center energies of 3 energy band. Even after that, the comparison of the PIN NXB spectrum between the earth data and the model has an energy-dependent systematic residual at $\sim 2\%$, and thus we corrected it furthermore by a 4th order polynomial as a function of energy (the term $K_5(j)$ in the following formula). As a result, we obtain the PIN NXB light curve as,

$$BGD'_j(t) = BGD_{12-70\text{keV}}(t)K_1(COR, j)K_2(H_{\text{sa}}, j)K_3(\theta_{\text{elev}}, j)K_4(\theta_B, j)K_5(j)F(j)$$

where j is the pulse height channel of the PIN event, $BGD'_j(t)$ is the model count rate in the j -th pulse height channel, $BGD_{12-70\text{keV}}(t)$ is the model count rate in 12–70 keV band corresponding to $BGD_i(t)$ in §3.2.1, H_{sa} is a satellite altitude, θ_{elev} is an earth elevation, $K_{1,2,3,4}$ is a correction function, and $F(j)$ is a probability function of pulse height. In figure 7, the residual against the elevation angle for the corrected PIN NXB model is shown, demonstrating that the elevation dependence becomes reduced.

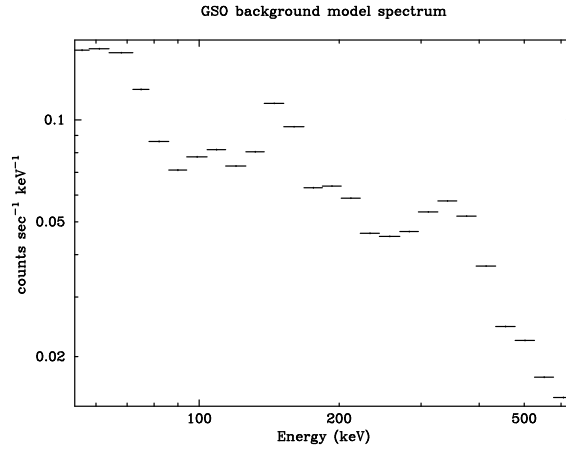


Fig. 6. An example of the GSO background model spectrum.

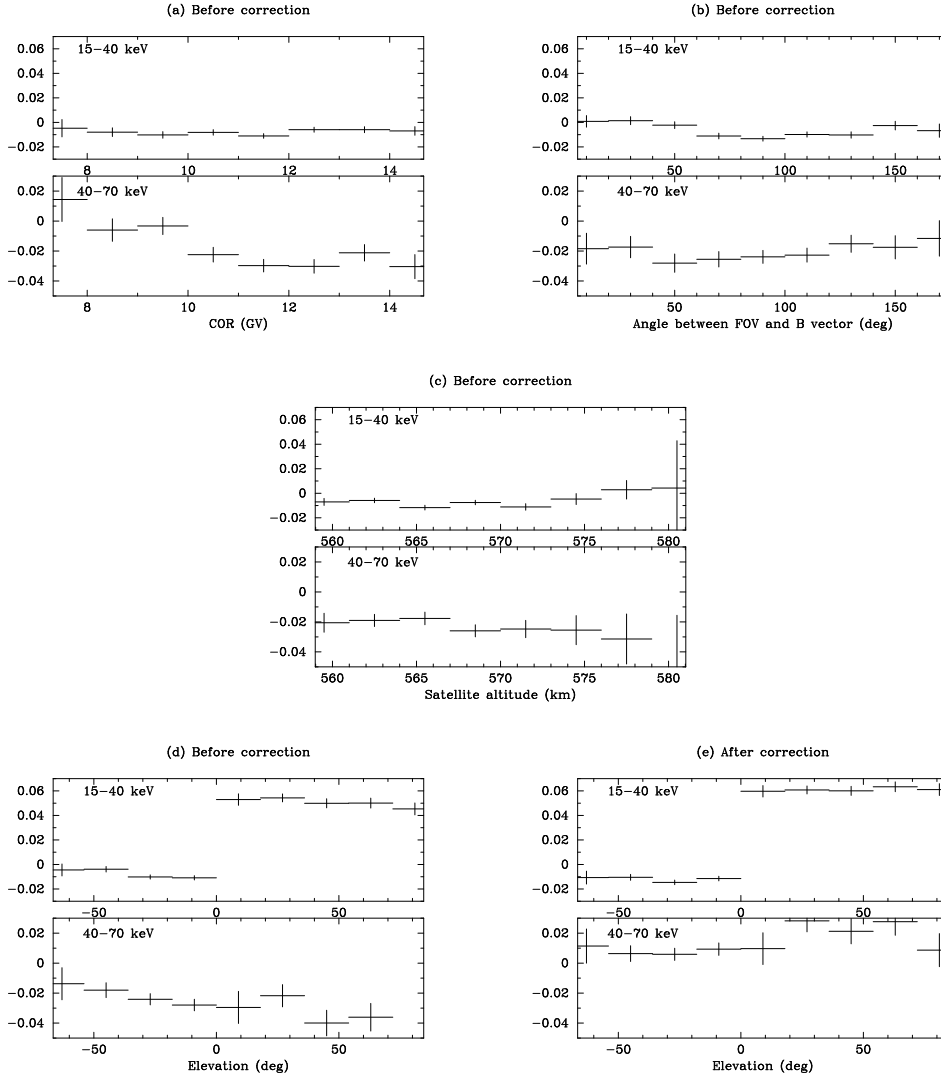


Fig. 7. The residual of PIN background subtraction against the (a) COR, (b) θ_B , (c) satellite altitude, and (e) earth elevation angle before the correction of background model. Exceptionally, the bottom-right figure (e) shows the residuals against the earth elevation after the correction of background model.

4. Reproducibility of the PIN NXB

4.1. Data Reduction

In this section, we examine the reproducibility of the NXB by utilizing the available sky and earth occultation data in 2005 Aug 17 to 2008 Jan 31 for the ver 2.0 pipeline processing. The event selection criteria are the same as those of cleaned event. To be specific, we applied the following selection criteria ⁶ : the COR is greater than 6 GV, the elapsed time after the passage of SAA (South Atlantic Anomaly) is more than 500 s and the time to the next entry to SAA passage is more than 180 s, high voltages from all eight HV units are in normal value, and the satellite is in pointing mode and the satellite attitude is stabilized. Elevation angle from the Earth rim is more than 5° or less than -5° for sky and Earth observation, respectively. We also use `hxdgtigen` to discard the time interval when the telemetry was saturated. Furthermore, the data and background for sky and earth observations are accumulated within the same good time interval (GTI).

4.2. Comparison with the earth occultation data

Here we show the reproducibility of both two PIN NXB models, by comparing the model with the earth occultation data. Although the background model is produced based on the earth data, the modeling is not complete, and therefore it is important to check how the modeling itself is accurate, before comparing the model with the sky data. Figure 8 compares energy spectra between the data and the NXB model during the Earth occultation of all available data (7.9 Ms exposure in total). We see a very good agreement between the model and the data, and can conclude that they agree within $\sim 1\%$ in 15–70 keV for the long-duration averaged Earth occultation data. Small but systematic deviation is seen below 20 keV.

For studying reproducibility in a shorter time scale, we split the Earth data in each target observation into small pieces with 10 ks exposure and compared the NXB count rate between the data and the model in 15–40 keV and 40–70 keV range as shown in figure 9 and 10, respectively, and the results are summarized in table 2. We see that the model reproduces the data in 15–40 keV within $\pm 7\%$. In figure 9, it is found that the reproducibility is somewhat worse for the PINUDLCUNIT in such a way that the model count rate is overestimated at higher background rate and the data to model ratio has a large scatter and gradually varies with time. More quantitatively, the average of the residual is -0.5% and -0.62% and the standard deviation is 3.75% and 2.31%, whereas the statistical error (1σ) is 1.83%, resulting in the systematic uncertainty of 3.27% and 1.40%, for PINUDLCUNIT and LCFITDT, respectively. Therefore, the systematic uncertainty of the LCFITDT “tuned” model is less than half of that

⁶ In the Suzaku analysis software, the criteria are given as `COR>6` and `(T_SAA_HXD>500 and TN_SAA_HXD>180)` and `(HXD_HV_W[0123]_CAL>700 and HXD_HV_T[0123]_CAL>700)` and `(AOCU_HK_CNT3_NML_P==1 and ANG_DIST<1.5)` and `(ELV>5 or ELV<-5)`

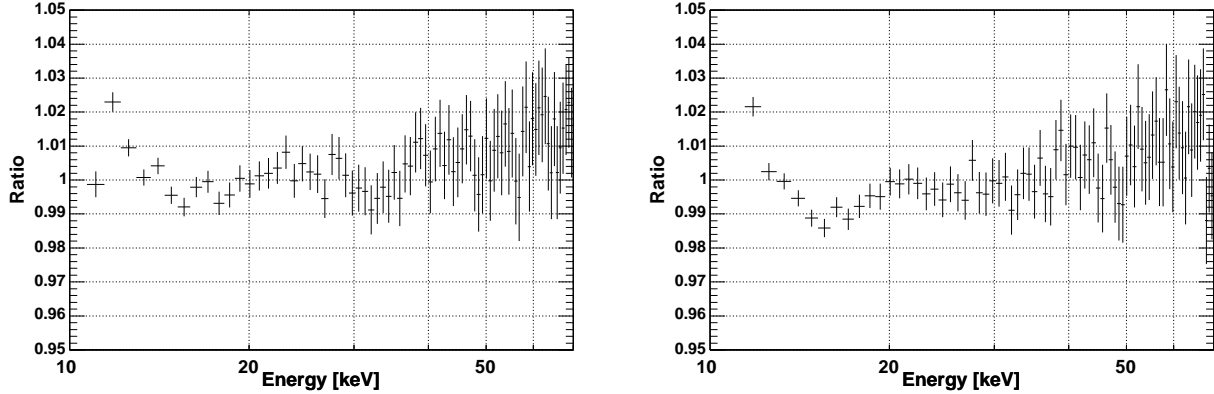


Fig. 8. Ratio of spectra between the data and the background model prediction of all the available Earth occultation data (7.9 Ms exposure). Left and right panels show the plots for PINUDLCUNIT and LCFITDT, respectively.

by the PINUDLCUNIT “quick” model, and the statistical error now dominates the residual for the LCFITDT model. We understand the negative mean of the residual for both models is due to the “dip” around 15 keV in figure 8. On the other hand, the statistical error dominates the residual in 40–70 keV: the average of the residual is 1.13% and 0.81% and the standard deviation is 5.53% and 4.92% for PINUDLCUNIT and LCFITDT, respectively, where the statistical error is 4.03%. Therefore, the standard deviation of residuals in high energy band is dominated by statistical errors.

In order to investigate the reproducibility for the LCFITDT method by avoiding the statistical error, we did the same comparison but with a longer integration time of 40 ks as summarized in table 2 and figure 11. As a result, the average, the standard deviation, and the statistical error of residuals in 15–40 keV is -0.58%, 0.99%, and 0.93%, respectively. This results in the systematic uncertainty of about 0.34%. For 40–70 keV, the average of the residual is 0.70% and the standard deviation and the statistical error is 2.87% and 2.03%, respectively, resulting in the systematic uncertainty of about 2.02% which is comparable to the statistical error.

4.3. Comparison with the data of dark objects

In the previous subsection, we confirmed that the background modeling is accurate by several percents for the earth occultation data. As described in §3.2.3, we consider that the background rate somewhat depends on whether the pointing direction is toward the sky or the earth. Although we include this effect into the model, we must check it. We therefore assess the NXB reproducibility by utilizing the sky observation with no apparent strong hard X-ray objects below.

We first utilized the XIS FI data to select observations with no strong X-ray emission in 7–12 keV (less than 20% above the XIS-FI NXB in entire XIS field-of-view) and compared

Table 2. Standard deviation (1σ) of residuals between the PIN earth data and model.

15–40 keV	10 ks		20 ks		40 ks	
	PINU DLCUNIT	LCFITDT	PINU DLCUNIT	LCFITDT	PINU DLCUNIT	LCFITDT
Standard deviation (σ)	3.75%	2.31%	3.23%	1.72%	2.96%	0.99%
Statistical error (σ_{stat})	1.83%		1.36%		0.93%	
Systematic error (σ_{sys})	3.27%	1.40%	2.93%	1.05%	2.81%	0.34%
40–70 keV	10 ks		20 ks		40 ks	
	PINU DLCUNIT	LCFITDT	PINU DLCUNIT	LCFITDT	PINU DLCUNIT	LCFITDT
Standard deviation (σ)	5.53%	4.92%	4.34%	3.51%	3.39%	2.87%
Statistical error (σ_{stat})	4.03%		3.01%		2.03%	
Systematic error (σ_{sys})	3.78%	2.82%	3.12%	1.81%	2.71%	2.02%

$\sigma_{\text{err}} = \sqrt{\sigma^2 - \sigma_{\text{stat}}^2}$

the HXD-PIN data and the NXB model count rate (10 ks exposure) in 15–40 keV, as shown in figure 12. Here we plotted the residual histogram in unit of count rate, not the ratio to the NXB model, since we expect a constant excess above 0 due to the CXB emission. The standard deviation (including statistical error) of the residual is about 5.0% and 3.5% of the mean NXB count rate for PINU DLCUNIT and LCFITDT, respectively, which are somewhat larger than that obtained from the Earth occultation data.

One possibility is that the systematic uncertainty increases when observing the sky, but the source confusion limit or fluctuation of the CXB must be considered before concluding. The source confusion limit is estimated from the logN-logS relation in the hard X-ray band. Based on the logN-logS relation obtained with the *INTEGRAL* (Beckmann et al. 2006), the source confusion limit for the PIN field of view becomes $8 \times 10^{-13} \text{ erg s}^{-1} \text{ cm}^{-2}$ (10–50 keV) at 3σ level, at most 0.08% of the PIN NXB. The CXB sky-by-sky fluctuation is calculated by scaling the HEAO-1 result of 2.8 % with the equation $\sigma_{\text{CXB}} \propto \Omega^{-0.5} S^{0.25}$ (Condon 1974), where $\Omega = 15.8 \text{ deg}^2$ and $S \sim 8 \times 10^{-11} \text{ ergcm}^{-2}\text{s}^{-1}$ are the effective solid angle of the observation and upper cut-off flux of the detectable discrete sources in the field of view, respectively. In the case of the HXD ($\Omega = 34' \times 34'$, and $S \sim 8 \times 10^{-12} \text{ ergcm}^{-2}\text{s}^{-1}$), the sky-to-sky fluctuation of the CXB is calculated to be 11% (1σ) of CXB flux, and therefore may not affect the reproducibility of the NXB since 1σ CXB fluctuation corresponds to at most $\sim 0.7\%$ of the PIN NXB, and then a larger standard deviation of the residual between data and model for the sky observation is not fully resolved. As a result, a standard deviation for 10 ks sky observations for the PIN 15-40 keV band becomes 2.9%, after subtracting the contribution of statistical error and CXB fluctuation. This is still larger than that for the earth data. Therefore, the reproducibility of the NXB model seems worse for sky observations, but one possibility is that the data selection based on the XIS could include the source with $> 0.2 \text{ mCrab}$ (2% of the PIN NXB in 15–40 keV) and such data could contribute to the standard deviation.

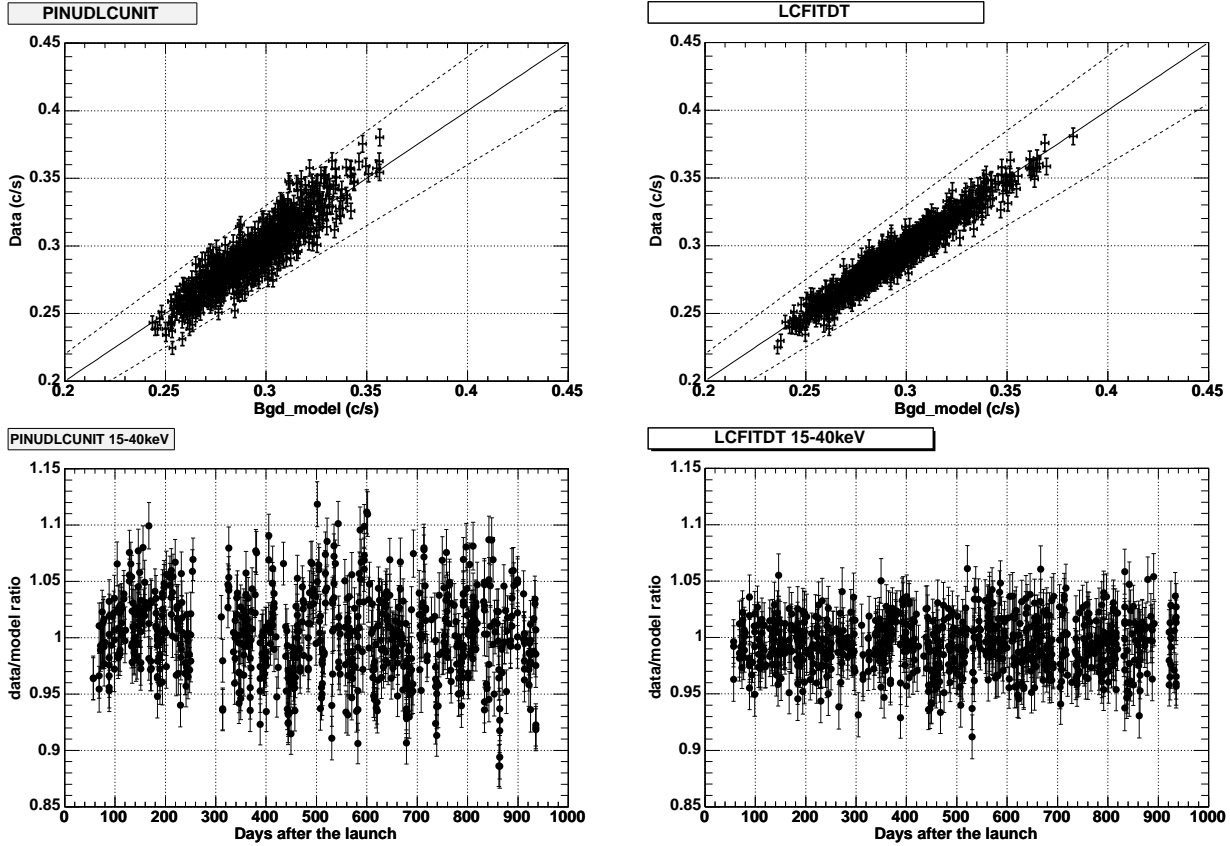


Fig. 9. Comparison of the NXB count rate in 15–40 keV between the data and the model prediction. Left and right panels show the plots for PINUDLCUNIT and LCFITDT, respectively. Top panels show a scatter plot between the NXB data and the background model. Bottom panels show data to model ratios of the NXB count rate, plotted against the day since 2005 July 10 (the day of Suzaku launch).

In order to avoid the possible CXB fluctuation sky by sky and source confusion observation by observation, we utilized the data of objects which have been repeatedly observed. Figure 13 shows the comparison between the sky data and the NXB model for the SNR E0102.2-7219 observations, in which the same region of the sky is observed regularly for the XIS calibration purpose. The X-ray emission from this source is thought to be constant and dark for the HXD-PIN, but some observations do not satisfy the selection criteria written at the beginning of this subsection, possibly due to sources or diffuse emission in the SMC within the XIS field-of-view, as reported by Takei et al. (2008). Different roll angle of the field of view against the SMC may also cause the difference of count rate among observations. Yet, we used all E0102.2-7219 observations in order to compare sky data and the NXB model of as many observations as possible. We also plotted the data and the NXB model of the Cygnus Loop multi-pointing observations in red. These observations were performed for the XIS calibration and cover the regions within 1.5 degree in radius, and thus the CXB fluctuation within the field of view of the HXD-PIN can be reduced.

We see a clear difference of the residual between two sets of observations. The difference

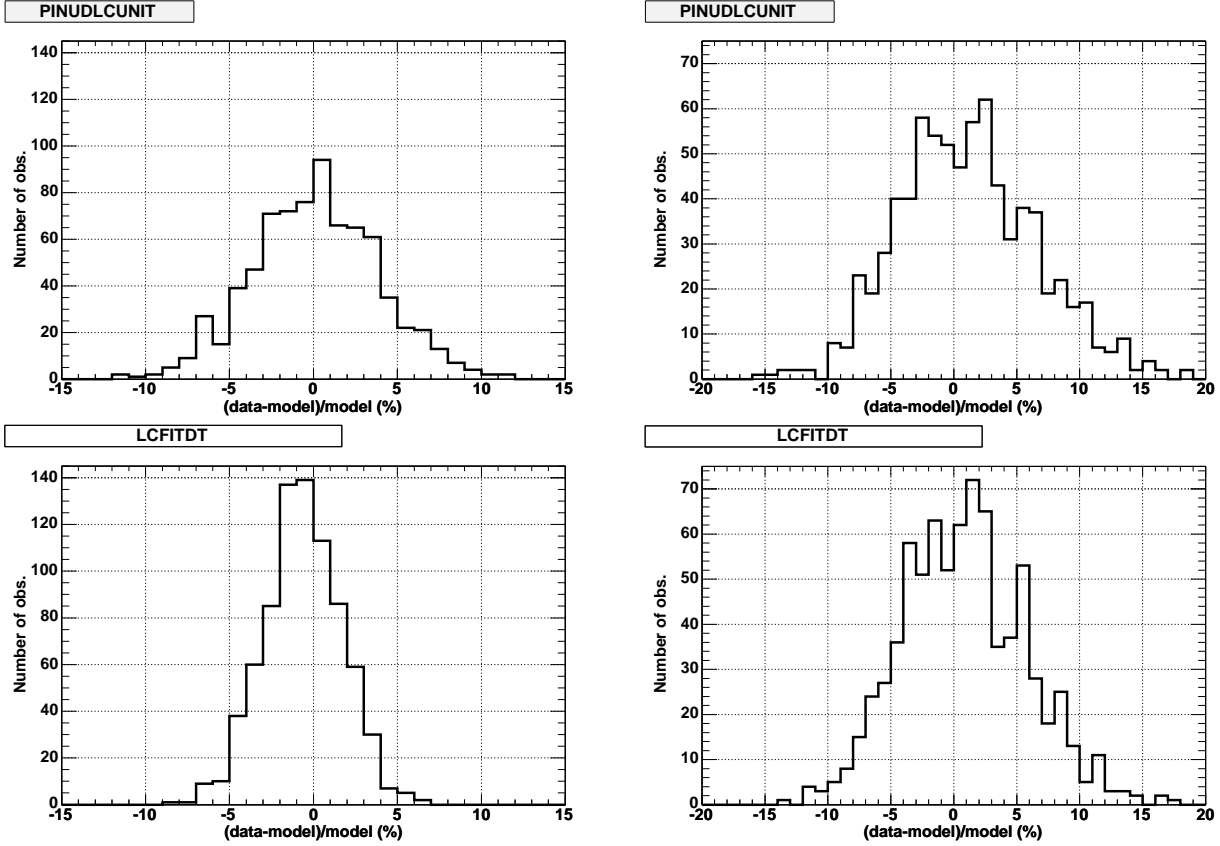


Fig. 10. Histograms of the fractional residual between the NXB data and background model. Top and bottom panels show the plots for PINUDLCUNIT and LCFITDT, respectively. Left and right show the plots for 15–40 keV and 40–70 keV, respectively.

of residuals between two data sets by $0.01\text{--}0.015\text{ c s}^{-1}$ could be due to a weak hard X-ray emission inside the PIN field-of-view of E0102.2-7219 observations. We look at a Swift/BAT archival image ⁷, but no significant sources with 0.3 mCrab (0.02 c s^{-1} for PIN) are found. Since this region is in the SMC, many candidates of hard X-ray sources exist, and a sum of their flux would explain the above excess flux.

From figure 13, the residual for E0102.2-7219 data concentrates around 0.03 c s^{-1} with a narrower width than that for all the dark objects in figure 12, but a few observations show an extraordinary small residual below 0.01 c s^{-1} . A standard deviation of the residual, including statistical errors, is 0.0080 c s^{-1} and 0.0077 c s^{-1} (2.7% and 2.6% of the mean NXB rate) for E0102.2-7219 and Cygnus Loop, respectively. This is smaller than that obtained from many dark observations, but somewhat larger than that for the earth observations. Three data points below 0.015 c s^{-1} for E0102.2-7219 are from observation on Feb. 10–11, 2007, and thus NXB accuracy is not good around this observation. As noted in §6, it was found that the NXB model

⁷ <http://skyview.gsfc.nasa.gov/>

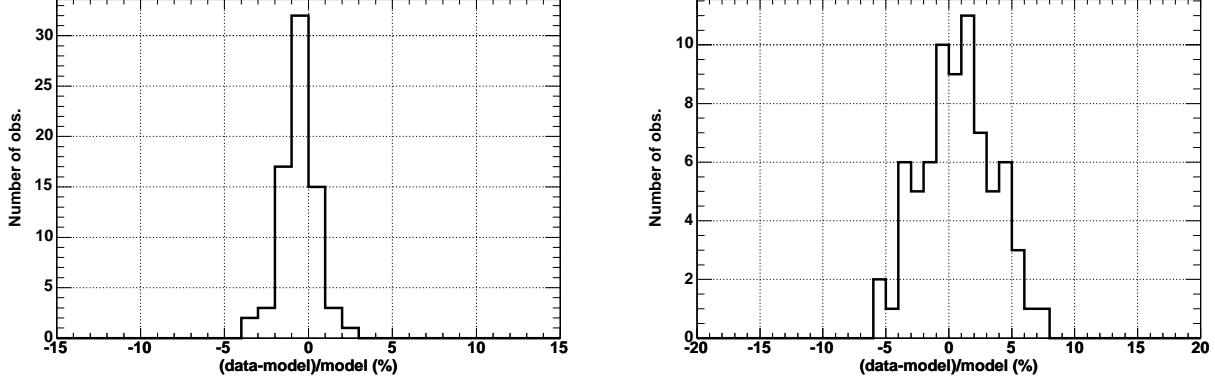


Fig. 11. The same plots for the LCFITDT at those of Figure 10, but the integration time is 40 ks instead of 10 ks. Left and right show the plots for 15–40 keV and 40–70 keV, respectively.

accuracy is not good for specific periods. In addition, four Cygnus Loop observations were performed in May 2006, when the background accuracy is relatively worse because the HXD operation mode was changed several times (§2.2). When excluding these data, the standard deviation becomes 2.3% and 2.1% of the mean NXB rate for E0102.2-7219 and Cygnus Loop, respectively, and these values are almost similar to that for the earth observations. Therefore, the PIN NXB background accuracy is almost the same between earth and sky observations in most cases. We return to this issue in §6.

Next, we investigate the accuracy of background-subtracted spectra by referring to the CXB. If we assume that the Cygnus Loop regions are free from any weak hard X-ray emission, we can regard the averaged spectrum as a sum of the CXB plus the NXB. The NXB-model-subtracted spectrum is compared with the spectrum of the CXB model by Boldt (1987) in figure 14. We see a very good agreement between the subtracted spectrum (green crosses) and the CXB model (blue ones) within 1% error.

In order to check the NXB reproducibility in a single observation, we also compared the spectrum and the light curve of objects whose signal is expected to be negligible for the HXD-PIN. Example of comparison of spectra are shown in Figure 15 left. The background-subtracted spectrum and the CXB model by Boldt (1987) is given in blue and green histograms, respectively. No systematic difference is seen between them up to 60 keV. Figure 15 right also compared the light curves between the data and the NXB model in 15–40 keV band with a time bin of 10 ks. Residuals are consistent with the CXB level in $\pm \sim 0.02 \text{ c s}^{-1}$, or $\sim 7\%$ of the total NXB count rate.

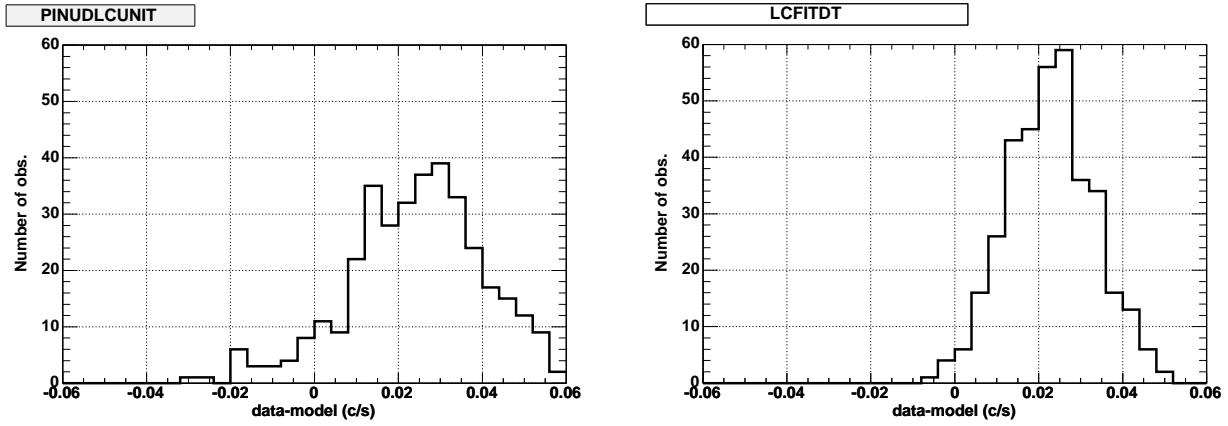


Fig. 12. Histogram of the residual count rate in 15–40 keV between the data and the NXB model for sky observations with 10 ks integration time. Observations with no apparent hard X-ray objects in XIS FOV are selected (see text for details of the data selection). Left and right panels show the plots for PINUDLCUNIT and LCFITDT, respectively.

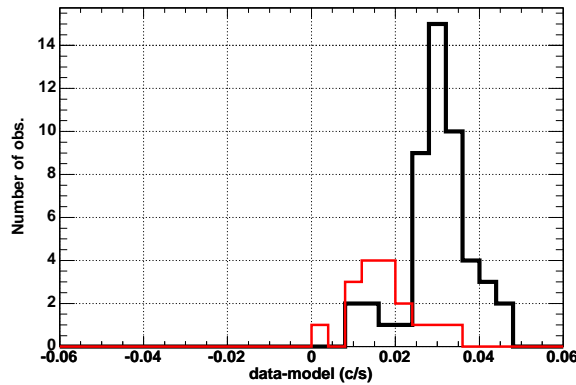


Fig. 13. The same as Figure 12, but observations of E0102 (black) and Cygnus LOOP multi-pointing (red) are used and results for the background model LCFITDT are shown.

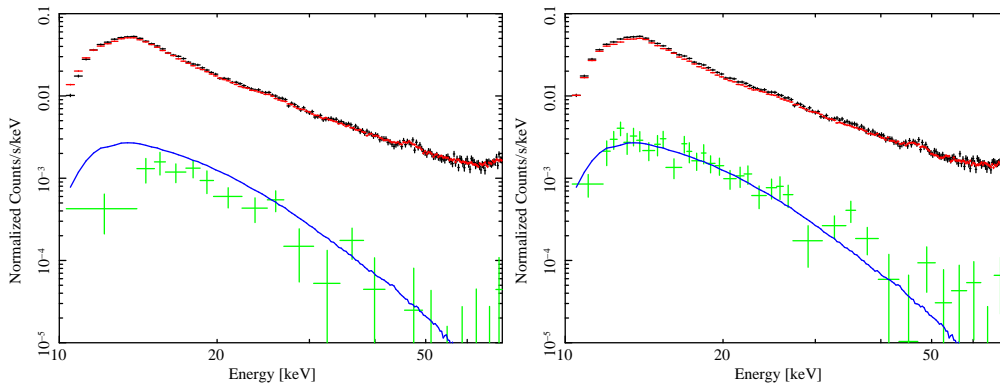


Fig. 14. Averaged spectra of sky observations (black) and the NXB model (red) of Cygnus LOOP multi-pointing observations, together with the subtracted spectrum (green) and the CXB model (blue) by Boldt (1987). Top and bottom panels show the plots for PINUDLCUNIT and LCFITDT, respectively.

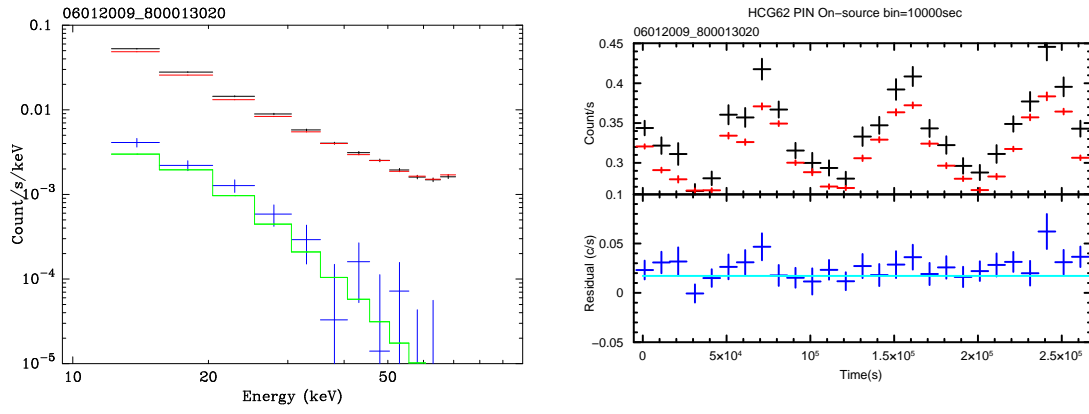


Fig. 15. Left panels are comparison of spectra between the data (black) and BGD model LCFITDT (red) for observation of HCG 62, which is thought to contain no known strong hard X-rays. Blue cross data points are residuals after the BGD model is subtracted, and the green solid line indicates a typical CXB spectrum. Right figure is the comparison of the light curve in 15–40 keV between the data (black) and BGD model LCFITDT (red) for observation of HCG 62. The bottom panel shows the residuals. A time bin is 10000 sec. The horizontal line in the bottom panel indicates the CXB level.

5. Reproducibility of the GSO NXB

5.1. Data Reduction

The data reduction is almost the same as the check of the PIN NXB, but we discard the period when the total GSO count rate is less than 15 cts sec^{-1} . Such a low count rate occurs when only 1/4 of GSO data are output to the telemetry for reducing the data size, usually during the data rate L (usually during SAA, low COR period, or earth occultation). However, this 1/4 mode sometimes continues even in the regular observation period ⁸, and becomes contained in the clean event. The background model does not support such a mode.

5.2. Comparison with the Earth Occultation Data

Each observation is divided into several periods during which the exposure is 10 ks. When the exposure of earth occultation within one observation is less than 10 ks, we do not use the data. Accordingly, the GSO count in each data set is typically $(4 - 9) \times 10^4$, and thus the statistical error is typically 0.3–0.5 %. In Figure 16, we compared the NXB count rates in each data set between the earth occultation data and the background model in 50–100 keV and 100–200 keV range, against the elapsed day after the Suzaku launch.

Most of the data and model agree within $\sim 2 \%$ with no time dependence, and no significant difference in reproducibility is seen between models even in the period of 2006 March 23 to May 13 during which the GSO LD level was changed. There are some data points, which significantly deviate from 1.0 by $>2\%$, corresponding to observations during which the HXD observation mode is not nominal and the background model cannot be applied. Figure 17 plots the distribution of the NXB count rate ratio between the data and the model prediction. In both energy band, the distribution is well represented by a Gaussian with σ of 0.72 % and 0.59 % in the 50–100 keV and 100–200 keV band, respectively. Considering the average of statistical error of 0.40 % and 0.36 %, the 1σ systematic error is estimated to be 0.60 % and 0.47 % in the 50–100 keV and 100–200 keV band, respectively. Note that the systematic error depends on the event selection criteria (e.g. COR and energy band) and the integration time. Table 3 summarizes a standard deviation in each energy band as a systematic error. There is an energy band dependency, but the systematic error is less than 1% at 1σ level in any energy band.

Figure 18 left shows the comparison of the spectra for earth data and background model, summed over 88 observations of dark objects. The total exposure is 923 ks. It can be seen that the data and model well agree with each other in all the energy band within 1 %.

5.3. Comparison with the Data of Dark Objects

In this section, we compared the NXB model with the sky data of dark objects, whose signal is expected to be negligible for the HXD-GSO. Example of comparison of spectra for dark

⁸ Data rate is medium or high or superhigh

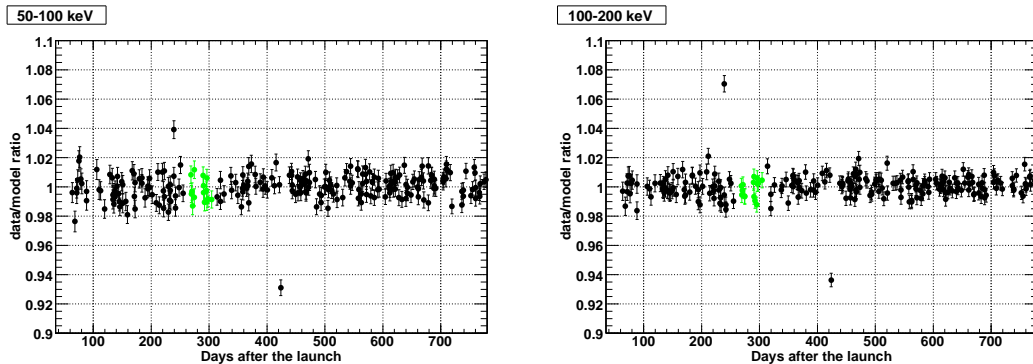


Fig. 16. (left) A comparison of the NXB count rate in the earth occultation in 50–100 keV between the data and the model prediction. Data from 2006 March 23 to May 13 are shown by green crosses (see text). (right) The same plot but for 100–200 keV.

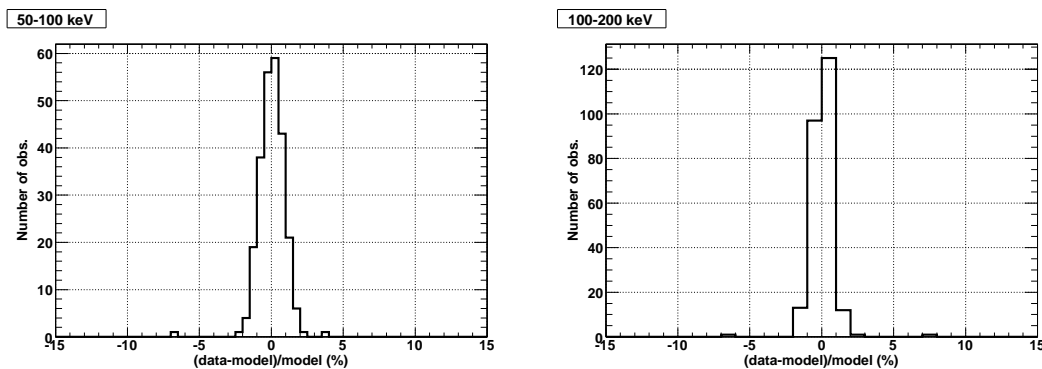


Fig. 17. (left) Distribution of fractional residual of the NXB count rate between the data and the model prediction in the 50–100 keV band. (right) The same plot but for the 100–200 keV band.

Table 3. Standard deviation (1σ) of residuals between the GSO earth data and model in each energy band.

	50–100 keV	100–200 keV	200–300 keV	300–500 keV
Standard deviation (σ)	0.72%	0.59%	0.87%	0.71%
Statistical error (σ_{stat})	0.40%	0.36%	0.46%	0.34%
Systematic error (σ_{sys})	0.60%	0.47%	0.74%	0.63%

$$\sigma_{\text{err}} = \sqrt{\sigma^2 - \sigma_{\text{stat}}^2}$$

objects are summarized in Figure 19 left. Unlike the PIN, the CXB is negligible in the GSO band. No systematic difference is seen between the data and BGD model spectra, indicating that the background model is applicable for sky observations. We also compared the data and the NXB model light curves as shown in figure 19 right. for the 50–100 keV band with a time bin of 4000 sec. Residuals are mostly within 2 % of the total count rate, and we see some modulations of a peak-to-peak amplitude up to $\sim 0.1 \text{ c s}^{-1}$ in a cycle of ~ 1 day.

Figure 18 right shows the comparison of the spectra for on-source data and background

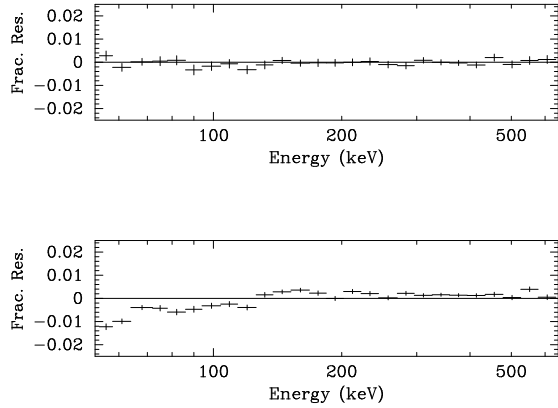


Fig. 18. Fractional residual of the spectra after subtracting the GSO background model from the earth data (top) and the sky data (bottom), summed over 88 observations of dark objects.

model, summed over 88 observations of dark objects. The exposure is 2430 ks. Although systematic difference is seen between the data and the model, they agree with each other within 1% in the whole energy band.

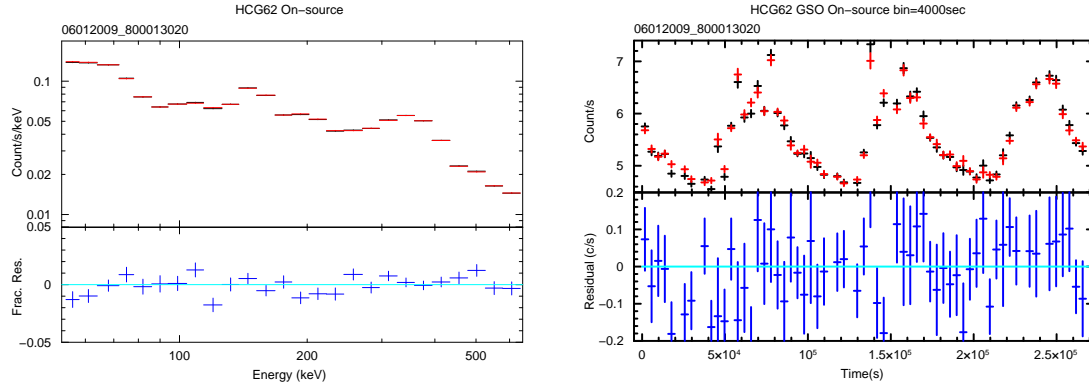


Fig. 19. The left figure is a comparison of spectra between the data (black) and BGD model (red) for observation of HCG 62 whose sky region contains no known strong hard X-rays. Fractional residuals are given by blue crosses in the bottom panel. Right figure is a comparison of the light curve in 50–100 keV between the data (black) and BGD model LCFITDT (red) for observation of HCG 62. The upper panel shows the light curve and the lower panel shows the residual. A time bin is 4000 sec.

6. Cause of Current Systematic Errors of the BGD model

Although we have developed the background model as accurately as possible, it does not completely reproduce the NXB. This may cause the issues described in §4.3; background reproducibility is not good for some specific observations. For studying the BGD systematic error related with this issue, it is very useful to investigate the background-subtracted light curve of the count rate in several ten days. Figure 20 shows light curves of fractional residual of count rate after subtracting the background model in 15–40 keV and 70–100 keV for PIN and GSO, respectively. Data of both on-source and earth-occultation are plotted as different colors for the GSO data. We do not show the on-source data for the PIN, since the PIN data contain the CXB signal and also often the target signal, and they are not useful for studying the BGD systematics. Together with the light curve of a shorter time scale in figure 19, it can be seen that the BGD systematic uncertainty is composed of two components; one with a shorter time scale within 1 day and another with a longer time scale of >1 day. The latter uncertainty appears as a modulation with a time scale of several days in the residual light curve, and its behavior is common between on-source and earth data. This behavior is clearly seen for the GSO. For the PIN, the modulation is a less clear but significant modulation at several percents exists. This trend is also found for the PIN NXB-subtracted light curve around the E0102.2-7219 observation on Feb. 10–11, 2007, leading to somewhat worse reproducibility as described in §4.3.

Accordingly, by studying the light curve as above, the background level is more accurately determined than by simply subtracting the background model. As can be seen from the trend in figure 20, the reproducibility is generally worse around the observation during which earth occultation data are not available for >1 days. This is because the NXB modeling refers to the earth data. This trend could be smaller when sky observations with no significant PIN/GSO signal are utilized for the NXB modeling. Since celestial GSO signal is negligible in most of observations, the choice of sky observations is not difficult for the GSO NXB modeling. On the other hand, this is not the case for the PIN, the choice of sky observations must be paid much attention to.

Apart from the above issue, for the GSO NXB, the elevation dependence of $\sim 1\%$ has been found below 70 keV as shown in figure 21. Although the dependence is very small, we will include such dependence into the GSO NXB model as the PIN NXB model in the near future. This will improve the systematic negative residual in the low energy band in figure 18.

7. Current Sensitivity of the HXB

As described in the previous sections, the current HXD NXB modeling achieves 1–3% reproducibility, but this accuracy depends on the integration time, energy band, period, and so on. Generally, a shorter integration time or a narrower energy band introduce a larger statistical

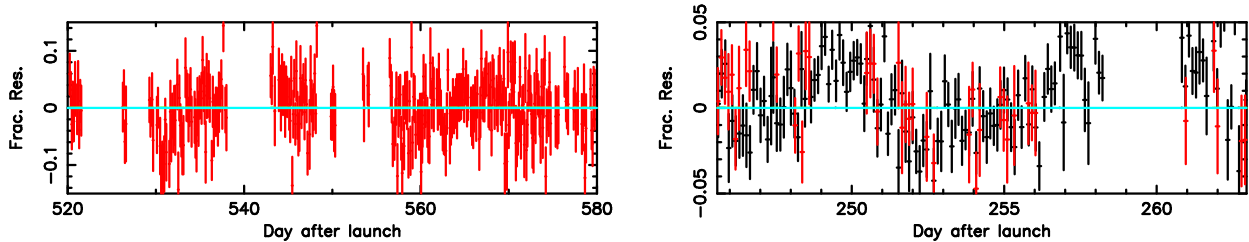


Fig. 20. Light curve of fractional residual of count rate after subtracting the background model in 15–40 keV and 70–100 keV for the PIN (left) and GSO (right), respectively. Black and red represent the residual of on-source data and earth data, respectively.

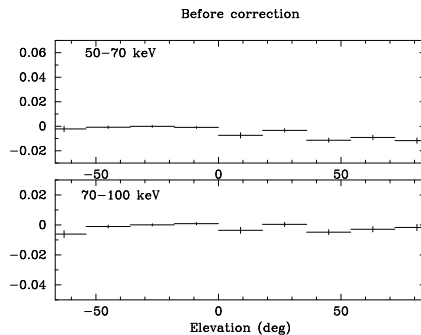


Fig. 21. The residual of GSO background subtraction against the earth elevation angle.

error, and thus the accuracy of the NXB subtraction is limited by the photon statistics of the background count rate. Figure 22 shows a comparison of the sensitivity limited by the systematic and statistical errors. Since the PIN-NXB count rate is very low, the statistical error becomes dominant for a shorter integration time. On the contrary, the GSO sensitivity is almost determined by the systematic error. Note that this figure represents the sensitivity in a wide energy band ΔE of $0.5E$ at a given energy E for a 100 ks exposure. In the spectral analysis, the spectral bin size often corresponds to narrower energy band, and thus the statistical error in each spectral bin is larger. Furthermore, the PIN sensitivity is also dependent on the CXB sky-to-sky fluctuation, which is similar level to the current PIN-NXB reproducibility.

8. Summary

We modeled the HXD PIN/GSO NXB by utilizing several parameters, including particle monitor counts and satellite orbital/attitude information. Current reproducibility of the NXB model is estimated to be less than 3% (PIN 15–40 keV) and 1% (GSO 50–100 keV) for more than 10 ksec exposure. The reproducibility is generally worse around the observation during which no earth occultation data are contained.

The authors wish to thank all members of the Suzaku Science Working Group, for their contributions to the instrument preparation, spacecraft operation, software development, and

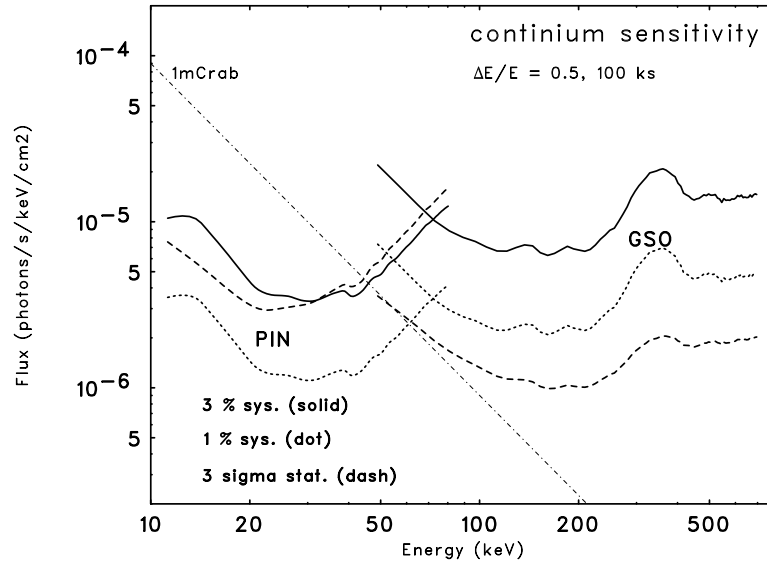


Fig. 22. Continuum sensitivity of the HXD. The solid and dot lines represent the sensitivity limited by the systematic error of the NXB modeling at 3% and 1% accuracy, respectively. The dashed line represents the sensitivity limited by the statistical error for 100 ks observation.

in-orbit calibration. This work is partly supported by Grants-in-Aid for Scientific Research by the Ministry of Education, Culture, Sports, Science and Technology of Japan (1479206 and 1479201).

References

- Beckmann, V., Soldi, S., Shrader, C. R., Gehrels, N., & Produitt, N. 2006, *ApJ*, 652, 126
- Boldt, E. 1987, *IAUS*, 124, 611
- Churazov, E. et al. 2007, *A&A*, 467, 529
- Churazov, E., Sazonov, S., Sunyaev, R., & Revnivtsev, M. 2008, *MNRAS*, 385, 719
- Condon, J. J. 1974, *ApJ*, 188, 279
- Frontera, F. et al. 2007, *ApJ*, 666, 86
- Hayashida, H., Inoue, H., Koyama, K., Awaki, H., & Takano, S. 1989, *PASJ*, 41, 373
- Imhof, W. L., Nakano, G. H., & Regan, J. B. 1976, *J. Geophys. Res.*, 81, 2835
- Jahoda, K. et al. 2006, *ApJS*, 163, 401
- Kokubun, M. et al. 1999, *IEEE Trans. Nucl. Sci.*, 46, 371
- Kokubun, M. et al. 2007, *PASJ*, 59, S53
- Mitsuda, K. et al. 2007, *PASJ*, 59, S1
- Sazonov, S., Churazov, E., Sunyaev, R., & Revnivtsev, M. 2007, *MNRAS*, 377, 1726
- Takahashi, T. et al. 2007, *PASJ*, 59, S35
- Takei, D., Tsujimoto, M., Kitamoto, S., Morii, M., Ebisawa, K., Maeda, Y., Miller, E. D. 2008, *PASJ*, 60, S231
- Tawa, N. et al. 2008, *PASJ*, 60, S11